

Artifacts identification in apertureless near-field optical microscopy

P. G. Gucciardi^{a)}

CNR-Istituto per i Processi Chimico-Fisici, sezione Messina, Via La Farina 237, I-98123 Messina, Italy

G. Bachelier

Laboratoire de Spectrométrie Ionique et Moléculaire, Université Claude Bernard Lyon I-CNRS (UMR 5579), 43 Bd du 11 novembre 1918, F-69622 Villeurbanne, France

M. Allegrini

Dipartimento di Fisica "E. Fermi," Università di Pisa, Largo B. Pontecorvo 3, I-56127 Pisa, Italy and polyLab CNR-INFM, Largo B. Pontecorvo 3, I-56127 Pisa, Italy

J. Ahn, M. Hong, S. Chang, and W. Jhe

Center for Near-Field Atom-Photon Technology, Seoul National University, Seoul 151-747, Korea and School of Physics, Seoul National University, Seoul 151-747, Korea

S.-C. Hong and S. H. Baek

Department of Physics, Korea University, Seoul 136-713, Korea

(Received 3 October 2006; accepted 3 January 2007; published online 20 March 2007)

The aim of this paper is to provide criteria for optical artifacts recognition in reflection-mode apertureless scanning near-field optical microscopy, implementing demodulation techniques at higher harmonics. We show that optical images acquired at different harmonics, although totally uncorrelated from the topography, can be entirely due to far-field artifacts. Such observations are interpreted by developing the dipole-dipole model for the detection scheme at higher harmonics. The model, confirmed by the experiment, predicts a lack of correlation between the topography and optical images even for structures a few tens of nanometers high, due to the rectification effect introduced by the lock-in amplifier used for signal demodulation. Analytical formulas deduced for the far-field background permit to simulate and identify all the different fictitious patterns to be expected from metallic nanowires or nanoparticles of a given shape. In particular, the background dependence on the tip-oscillation amplitude is put forward as the cause of the error-signal artifacts, suggesting, at the same time, specific fine-tuning configurations for background-free imaging. Finally a careful analysis of the phase signal is carried out. In particular, our model correctly interprets the steplike dependence observed experimentally of the background phase signal versus the tip-sample distance, and suggests to look for smooth variations of the phase signal for unambiguous near-field imaging assessment. © 2007 American Institute of Physics.

[DOI: [10.1063/1.2696066](https://doi.org/10.1063/1.2696066)]

I. INTRODUCTION

Apertureless scanning near-field optical microscopy (a-SNOM) is an extremely powerful technique capable of 10 nm spatial resolution,^{1,2} providing powerful means to probe the local fields around single nanoobjects such as metallic particles or nanowires.^{3,4} Apertureless SNOM has therefore attracted much interest, in view of the recent applications of such materials in high sensitivity spectroscopy,⁵⁻⁷ and as hybrid plasmonic light guides at visible frequencies.⁸ In a-SNOM a sharp metallic tip is scanned on top of the sample surface and the optical interaction on the local scale is monitored. The high performances of a-SNOM are, however, subject to the capability of suppressing the huge far-field background due to spurious reflections from the tip shaft and other sources that would overwhelm the tiny near-field scattering, and lead to fictitious optical images called artifacts. Such images do not provide any information on the optical properties of the sample, being a mere optical readout

of the topography. That is why they are also called z -motion artifacts. This phenomenon still represents a severe limitation to the applications of aperture SNOM to refractive-index imaging.⁹⁻¹¹ In apertureless SNOM, conversely, homodyne or heterodyne interferometric techniques can be used to augment the near-field signal. At the same time, the background can be reduced by vibrating the tip vertically at frequency ω and detecting the nonlinear part of the tip-sample interaction by means of lock-in demodulation at higher harmonics.¹²⁻¹⁴ Such technique is, however, not intrinsically background-free, since the movement of the tip introduces a far-field background component at every harmonic $n\omega$, whose intensity changes with the tip-sample distance.^{15,16} In particular, first harmonic demodulation is usually not capable of strong background suppression, especially in the visible range.^{12,17,18} Unambiguous artifact-free imaging is therefore achieved only in those experimental configurations in which it is possible to reject the far-field background below the detector's noise threshold. Such condition is usually well satisfied when operating in the midinfrared.^{19,20} In the visible range, where the physical properties of metallic nanoparticles

^{a)}Electronic mail: gucciardi@me.cnr.it

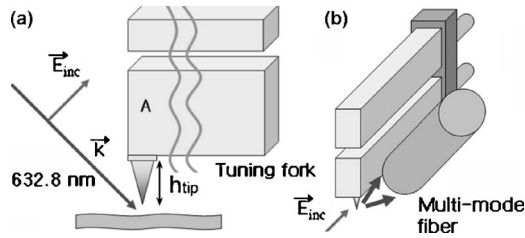


FIG. 1. Experimental setup: sketches (a) of the optical excitation and (b) of the light detection.

are of remarkable interest, the background signal can still be very intense, and its nonlinear dependence on the tip-sample distance can yield fictitious images difficult to identify as artifacts *a priori* even after homodyne amplification²¹ and demodulation at higher harmonics. In this paper we analyze the effects of a not perfect background rejection, in order to provide a coherent framework that helps to interpret the experimental results reported in the literature concerning the background at higher harmonics in reflection-mode apertureless SNOM. Developing the dipole image-dipole model^{22,23} for the higher harmonics detection, we simulate the typical fictitious patterns to be expected in the optical maps in presence of artifacts, comparing the results with experimental observations, and providing general criteria for artifacts identification for both the amplitude and the phase signals.

II. EXPERIMENT

Far-field artifacts have been experimentally evidenced by means of the setup sketched in Fig. 1. A HeNe laser beam ($\lambda=632.8$ nm, $P=450$ μ W) is focused on the tip through a long working distance objective (WD=10 mm), on a spot ~ 5 μ m wide. The incidence angle is 45° ; the light is p polarized [Fig. 1(a)]. Commercial atomic force microscopy (AFM) gold-coated tips (NT-MDT, CSG01/Au) are used having lengths (h_{tip}) in the micron range, ending with a radius of curvature of approximately 35 nm. The tip is glued on one prong of a tuning fork (TF), which oscillates vertically at resonance ($f\sim 32.7$ kHz), with a dithering amplitude $a_0=35$ nm (i.e., 70 nm_{pp}). Light collection is accomplished by means of a multimode optical fiber (core diameter 800 μ m) placed at a few millimeters from the tip. The fiber axis lies in a plane orthogonal with respect to the one defined by the TF prongs [Fig. 1(b)], and is inclined of $\sim 45^\circ$ with respect to the vertical. Light is detected by means of a photomultiplier tube (PMT) whose output is fed into a lock-in amplifier for demodulation at the different harmonics. The TF-tip assembly operates in a tapping-mode AFM framework. A personal computer (PC) drives the sample's scan, the tip-sample distance control, and the signals acquisition. No additional interferometric stages are present for the amplification of the near-field scattering.

The investigated sample is an Al-coated diffraction grating (NT-MDT, model TDG01) with a pattern height $\Delta z\sim 55$ nm and a period of 278 nm.

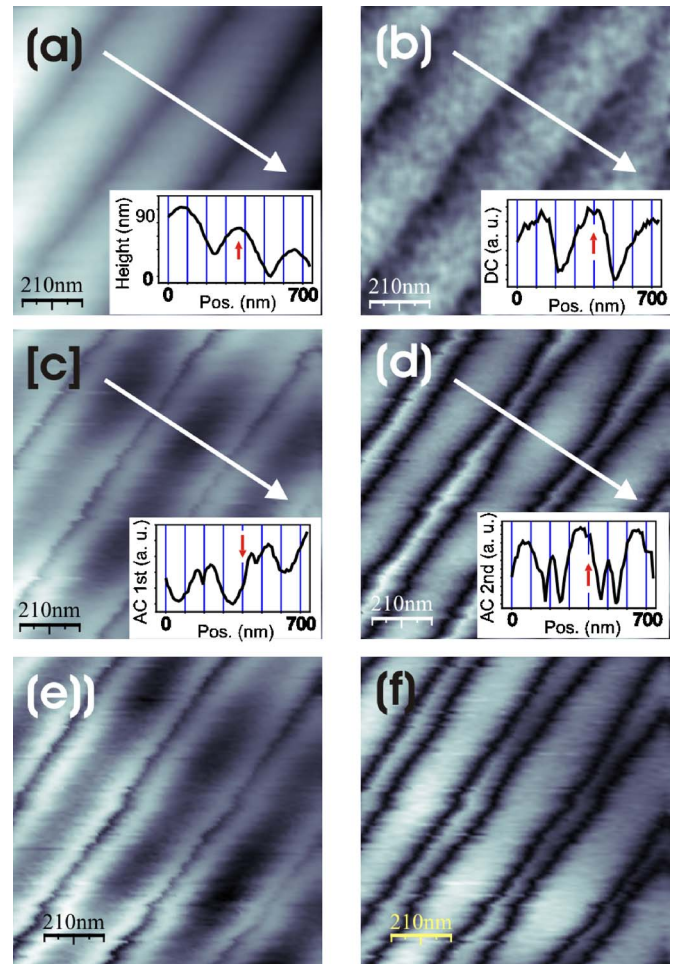


FIG. 2. (Color online) Experimental results with line profiles (insets) of the measurements carried out on an Al-coated grating. (a) Topography, (b) dc optical signal, (c) first harmonic optical signal, (d) second harmonic optical signal, (e) third harmonic signal, and (f) fourth harmonic signal.

III. RESULTS AND DISCUSSION

Figure 2 shows the topography [Fig. 2(a)] and the optical maps [Figs. 2(b)–2(f)] acquired on a 1.05×1.05 μm^2 portion of the metallic grating. Figure 2(b) is the dc map, Figs. 2(c)–2(f) are the signals demodulated at the first, second, third, and fourth harmonic, respectively. The insets represent the line profiles drawn along the white arrows. The topography shows the grating's periodic modulations (280 nm pitch, 55 nm height). A slight inclination of the grating's average plane ($\sim 4.5^\circ$) with respect to the horizontal scan plane is observed. We immediately note the strong similarity between the topography and the dc map, indicating the possible occurrence of a topography artifact. The slight lateral shift between the maxima in the topography and the dc line profiles (indicated by the red arrows) does not support the absence of artifacts according to the criteria valid for apertureless SNOM,^{9,24} since it is immediately lost when we remove the topography inclination by an average plane subtraction. The situation is completely different when looking at the optical maps demodulated at higher harmonics. Striking differences are visible between the maps acquired at the first and the second harmonic [Figs. 2(c) and 2(d), respectively]. The maps show the same periodicity of the grating, and the sec-

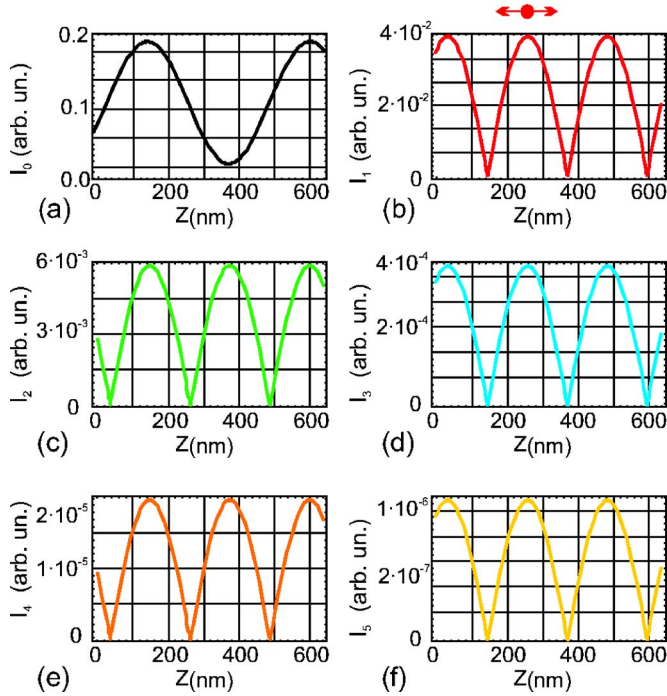


FIG. 4. (Color online) Approach curves simulated using the dipole-dipole model. We assume $h_{\text{tip}}=3.4 \mu\text{m}$ and a collection direction $\theta=\pi/4$. (a) dc optical signal [(b)–(f)] optical signals demodulated at the harmonic $n=1, \dots, 5$, respectively.

Moreover it will depend on the tip vibration amplitude a_0 , the wavelength (through k), and the collection angle θ . We recognize that the functional dependence of the odd harmonics on Δz is exactly the same, whatever the value of n . The same holds for the even harmonics. We can therefore assume the qualitative identity between the odd or the even harmonics as a criterion to assess the far-field nature of the detected signals, also for the reflection-mode configuration.

Equations (4) can be used to simulate the optical images expected for a grating topography $\Delta z(x, y)$ like the one measured in Fig. 2(a), by mapping the values of $I_n[\Delta z(x, y)]$ at each point of the sample. The unknown phase factor ϕ_0 is assumed as a free parameter. We note that the actual functions to be used in the calculations must take into account the rectification effect introduced by the lock-in amplifier on the harmonics, due to the fact that in real experiments the signal coming from the amplitude channel is monitored. Therefore the actual transfer functions will be

$$\begin{aligned}
 I_0(x, y) &= C + BJ_0(2ka_0 \cos \theta) \cos[\phi_0 + 2k \cos \theta \Delta z(x, y)], \\
 I_{2n}(x, y) &= 2B |J_{2n}(2ka_0 \cos \theta)| \cos[\phi_0 \\
 &\quad + 2k \cos \theta \Delta z(x, y)], \\
 I_{2n+1}(x, y) &= 2B |J_{2n+1}(2ka_0 \cos \theta)| \sin[\phi_0 + 2k \cos \theta \Delta z(x, y)].
 \end{aligned}
 \tag{5}$$

Equations (5) can be used to calculate approach curves $I_n(\Delta z)$ which, as we will see, allow us to visualize the characteristics of the far-field background discussed above. In Fig. 4 we report the approach curves expected for the dc signal [Fig. 4(a)] and the first five harmonics [Figs.

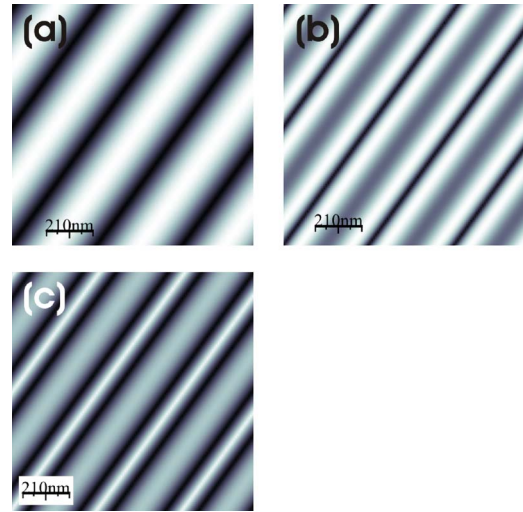


FIG. 5. (Color online) dc (a), first (b), and second harmonic (c) demodulated signals simulated for a topography structure equal to the one measured in Fig. 2(a).

4(b)–4(f)]. The phase ϕ_0 assumed for these calculations corresponds to a tip length $h_{\text{tip}}=3.4 \mu\text{m}$, and a collection angle $\theta=\pi/4$. The position $\Delta z=0$ corresponds to the tip-sample contact point, in which the feedback is engaged. While the dc signal shows a sinusoidal behavior with period $\lambda/(2 \cos \theta) \sim 448 \text{ nm}$, the periodicity of the harmonics signals is halved. The rectification effect introduced by the lock-in produces the humps visible in Figs. 4(b)–4(f). We see that the functions $I_n(\Delta z)$ are strongly nonlinear even on scales as small as $\Delta z \sim 50 \text{ nm}$. The shape of the odd (and of the even) harmonics is the same, apart from the absolute intensity which decreases with increasing n (the well known background suppression effect). We finally note that for this specific choice of ϕ_0 , the derivative of the signals at the contact point is positive for the dc and the odd harmonics [Figs. 4(a), 4(b), 4(d), and 4(f)] while it is negative for the even ones [Figs. 4(c) and 4(e)]. Therefore an increased topography will induce an increase of the optical dc and of the even harmonics signals, while for the odd harmonics the signal is expected to decrease, inducing a contrast inversion in the maps. The slope of the approach curves at the contact point is closely related to ϕ_0 , and therefore it is expected to change for different tip lengths or collection angles, as indicated by the arrows in Fig. 4. In general, contrast inversion could be observed also in dc or the first harmonic maps.

In Figs. 5(a)–5(c) we report the optical images $I_n[\Delta z(x, y)]$ for $n=0, 1$, and 2 , respectively, expected from the grating structure of Fig. 2(a). We immediately note the strong qualitative agreement between the experimental images in Figs. 2(b)–2(d) and the calculated ones, confirming the far-field nature of the observed signals. Since the optical maps are expected to strongly depend on the phase factor ϕ_0 , it is interesting to see the different optical patterns that a simple grating can provide. In Fig. 6 we report four images of the first harmonic signal, calculated increasing ϕ_0 of a few percent at each step. We observe a gradual transition between an image (a) similar to Fig. 5(b), to a picture (b) resembling the negative of the topography, to one (c) similar to the to-

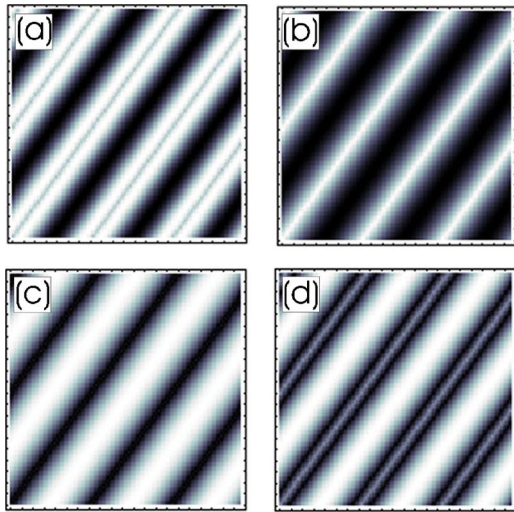


FIG. 6. (Color online) Different fictitious optical images ($n=1$) expected for a topography structure such as the one in Fig. 2(a), calculated for different values of ϕ_0 .

pography or, finally, to a map resembling the second harmonic one in Fig. 5(c). The completely different patterns arising from a simple grating structure as the one studied demonstrate the impossibility to carry out any genuine near-field imaging assessment through simple arguments based on qualitative differences between the optical and the topography maps. Equations (5) allow us to carry out rapid simulations of all the artifact-induced maps that are expected for a given topography structure, and compare them with the experiment in order to assess the true origin of the signals.

So far we have studied the dependence of the harmonic signals on z . We now focus our attention on the dependence of the signal strength on the oscillation amplitude a_0 and on possible far-field artifacts induced by a not perfect stabilization of a_0 during the scan. From Eqs. (5) we see that the amplitude of the far-field signals scales as $J_n(2ka_0 \cos \theta)$. In the small oscillation approximation, that is, for $2ka_0 \cos \theta \ll 1$, the first order Taylor expansion of the Bessel functions gives

$$I_n(a_0) \approx \frac{(2\pi \cos \theta)^n}{n!} \left(\frac{a_0}{\lambda}\right)^n. \quad (6)$$

The far-field signals are, therefore, characterized by a power dependence on the ratio a_0/λ . This is highlighted in Fig. 7 where we plot the amplitudes of I_n vs a_0 for the first five harmonics $n=0, \dots, 5$. Here we assume $\theta = \pi/4$ and $\lambda = 633$ nm. We immediately observe the decrease of the far-field signals with decreasing a_0 , as well as the enhanced rejection power of the higher harmonics for a fixed value a_0 . We moreover outline that increasing θ helps in suppressing the background due to the term $\cos^n \theta$. As an example, for an oscillation amplitude of 35 nm (yellow rectangle in Fig. 7) we expect the far-field background at the fifth harmonic to be smaller by a factor of 5×10^{-4} with respect to the first harmonic one. Equation (6) shows, as well, that any change Δa_0 around a fixed value a_0 is expected to produce a change of the optical signal

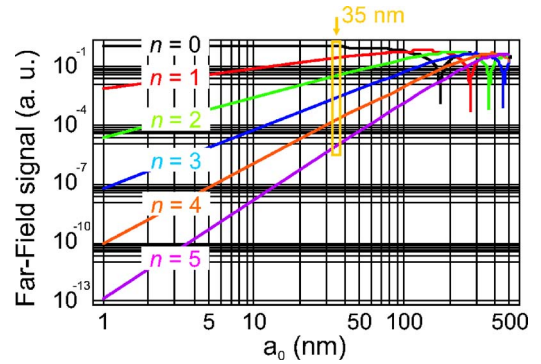


FIG. 7. (Color online) Plot of the far-field signal intensity as a function of the tip oscillation amplitude, calculated for the first five harmonics. The dips on the right hand side correspond to the first zeros of the Bessel functions.

$$\frac{\Delta I_n}{I_n} \approx n \frac{\Delta a_0}{a_0}. \quad (7)$$

That is, a relative tip-oscillation amplitude variation of 1% will influence the first harmonic signal by 1%, the second harmonic signal by 2%, and so on. Artifacts related to variations of the tip-oscillation amplitude have been recently put forward by Billot *et al.*³² on an a-SNOM apparatus using a tapping-mode AFM scheme for the tip-sample distance stabilization. Such artifacts, named “error signal artifacts” (ES artifacts), occur when the feedback does not react promptly to the presence of a topographic relief, in particular, when scanning too fast. The oscillation amplitude, in fact, changes when the tip encounters a relief, increasing on one edge and decreasing on the other, for a short delay of time before recovering the set point. As a consequence the optical signal will follow the actual value of a_0 , resembling the error map. Billot *et al.* have interpreted this effect by means of two-dimensional (2D) finite elements numerical methods, which usually mix up the near-field with the far-field information in the detected signal. Based on the observation made by the authors that “this kind of artifacts is prevalent when the laser is not well focused below the tip,” we suggest that the nature of ES artifacts could be related to the far-field component of the optical signals not properly rejected. To support our hypothesis we apply Eqs. (5) to simulate the optical map expected in correspondence to structures similar to the ones investigated by Billot *et al.* In particular, we have simulated the optical map demodulated at $n=1$, expected from a set of nanopillars 35 nm height [see Fig. 8(a) and the line profile in Fig. 8(d)]. To simulate the slow time response of the feedback loop we have assumed an increase of 1% of the tip oscillation amplitude on one edge of the pillar, and an equivalent decrease on the other edge. Figures 8(b) and 8(e) display the corresponding tip oscillation map, analogous to the error map measured experimentally, and a line profile along a single pillar. The resulting optical map shown in Fig. 8(c) shows a double effect: a contrast inversion, due to the negative slope at contact of the approach curve considered for the simulation (a typical z -motion artifact), plus the presence of overshoots and undershoots at the particles edges due to the tip oscillation amplitudes instabilities (the ES artifact). In particular Fig. 8(c) closely reproduces the experimental

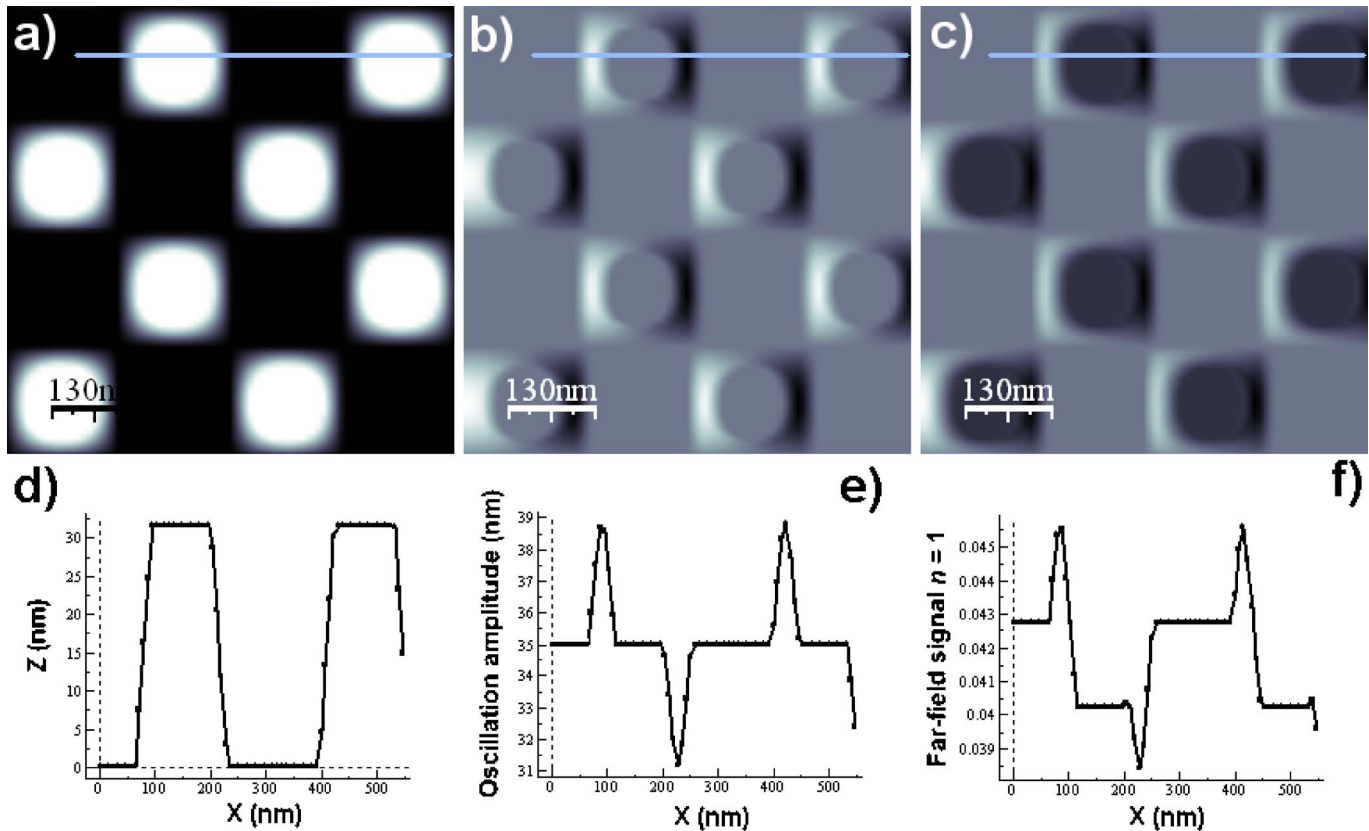


FIG. 8. (Color online) Topography (a), error map (b), and first harmonic optical map (c) simulated for 35 nm height nanoparticles (d), assuming a tip oscillation amplitude variation of 1% at their edges (e). The resulting optical signal shows contrast inversion, a typical fingerprint of z -motion artifacts, combined to the presence of overshoots and undershoots (f) induced by the ES artifact.

findings reported in Fig. 2 of Ref. 32 for gold nanoparticles. Finally, our model allows us to predict that ES artifacts are to be expected at every harmonic n , and that the relative optical signal variation is expected to be proportional to n .

As already pointed out for the transmission configuration,¹⁶ Eqs. (5) suggest the possibility to exploit the zeros of the Bessel functions, also for the reflection configuration, to null the far-field signal at a defined harmonic. If we oscillate the tip at an amplitude \tilde{a}_n such that the quantity $x_n = 2k\tilde{a}_n \cos \theta$ coincides with a zero of $J_n(x)$, in fact, the corresponding optical signal is expected to vanish. This, in particular, is evidenced in Fig. 7, where the dips on the right hand side of the figure represent the signal depletion due to this phenomenon. The presence of the term $\cos \theta$, however, tends to increase the values \tilde{a}_n as θ increases. For $\theta = \pi/4$, oscillation amplitudes larger than 250 nm (i.e., 500 nm_{pp}) are expected to null the signals demodulated at $n \geq 1$. Smaller values of \tilde{a}_n , more easily accessible from the experimental point of view, are expected for the backscattering configuration at $\theta = 0$. For this configuration, equivalent to the transmission mode one, values of \tilde{a}_n smaller than 200 nm are expected to null the background at $n = 0, 1$, and 2.

Up to now we have focused our attention on the amplitude signal. It is possible, however, to draw interesting considerations also on the phase signal induced by far-field artifacts. From the expansion of Eq. (3), we know that, in the small oscillation amplitude approximation, the analytical expression for the n th odd harmonic signal will be of the form

$$S_n = \left[2B \frac{(2\pi \cos \theta)^n}{n!} \left(\frac{a_0}{\lambda} \right)^n \right] [(-1)^n \sin(\phi_0 + 2k \cos \theta \Delta z)] \cos(n\omega t), \quad (8)$$

where the sine has to be replaced by a cosine if the even harmonics are considered. The phase signal measured in a real experiment by the lock-in corresponds the phase shift Φ_n between S_n and the reference $\cos(n\omega t)$. The factor in large brackets of Eq. (8) is a real positive quantity, therefore all the information on Φ_n is encoded in the term in small brackets $\Gamma = (-1)^n \sin(\phi_0 + 2k \cos \theta \Delta z)$. Γ , in particular, is always a real quantity which, depending on n and Δz , can be either positive and negative. Therefore, Φ_n is expected to depend on Δz in a steplike fashion assuming only two values: zero or π , depending on whether Γ is positive or negative. This fact is evidenced in the approach curve $\Phi_1(\Delta z)$ displayed in Fig. 9(a) (green line), calculated from Eq. (8). Here the phase signal demodulated at the first harmonic is plotted together with the amplitude [Fig. 9(a) (red line)], showing phase jumps of 180° in correspondence to the zero-crossing points of the amplitude signal. This behavior has been experimentally observed in approach curves performed at $\lambda = 10.6 \mu\text{m}$.²³ Phase values different from zero and π are expected in a real experiment for those values of Δz for which $I_n = 0$, where the phase is not defined and the corresponding signal gets extremely noisy.

It is now clear that far-field artifacts can be identified more easily by looking at the phase signal map rather than at

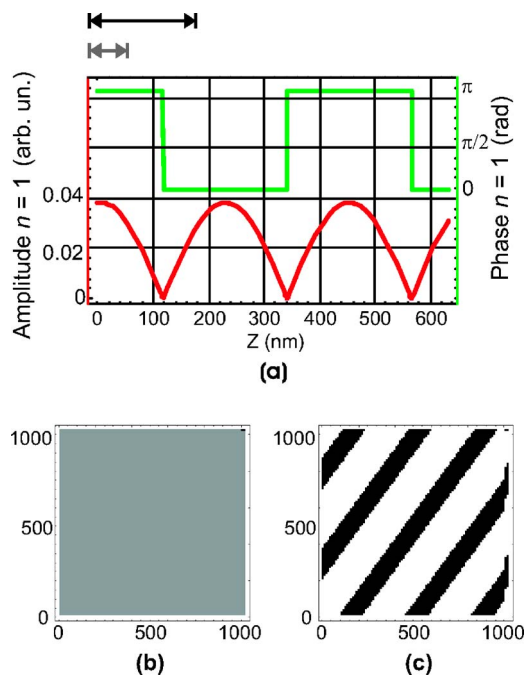


FIG. 9. (Color online) (a) Approach curves expected for the far-field amplitude (red line) and phase signals (green line) demodulated at the first harmonic. Optical phase maps expected for a 55 nm height (b) and for a 165 nm height grating (c). The arrows in (a) indicate the Z excursions corresponding to the two gratings.

the amplitude one. The far-field contribution to the phase signal is, in fact, a constant plateau, almost independent from the topography excursion, apart from discrete jumps of 180° . As an example, in Fig. 9(b) we have simulated the first harmonic phase signal maps expected for the metallic grating in Fig. 2(a) ($\Delta z = 55$ nm), and [Fig. 9(c)] for a grating structure three times higher ($\Delta z = 165$ nm). The first image is flat since the topography excursion [indicated by the shorter arrow in Fig. 9(a)] is not enough to induce a phase change. Vice versa, a 165 nm structure provides a vertical tip excursion [indicated by the longer arrow in Fig. 9(a)] is capable to induce the repeated phase change showing up in Fig. 9(c). This mechanism explains the experimental observations of Bek *et al.*³³ We finally note that, since Γ is independent from a_0 , no ES artifact has to be expected in the phase signal. In conclusion, only smooth changes of the phase signal measured in the approach curves close to the tip-sample contact point²⁰ or in the phase maps can be assumed as a criterion to assess a genuine near-field scattering.

IV. CONCLUSIONS

In this paper we have tried to answer two important questions in apertureless SNOM, namely, “which are the effects of the far-field background on the optical images” and “how can we identify if an optical image is affected by far-field artifacts.” To do this we have developed a theoretical model that describes the harmonic far-field background signal in the reflection configuration. In particular, it correctly interprets all those artifacts related to the vertical motion of the sample (z -motion artifacts) and to the tip oscillation amplitude variations (error-signal artifacts). We provide analytical formulas that allow us to quickly simulate and visualize

the set of the possible fictitious optical maps that can derive from a given topography, allowing the SNOM user to easily compare simulations with the experimental results, and conclude on the possible occurrence of artifacts. The model provides quantitative estimation of the background suppression power of higher harmonics demodulation as a function of the experimental parameters, suggesting at the same time the possibility to null the background by fine tuning the tip oscillation amplitude around some well defined discrete values. Finally, artifacts identification criteria are proposed. We show that artifacts produce amplitude maps that are identical at the different harmonics, a conclusion confirmed by the experiment. In addition we show that the phase signal, different from the amplitude, is not affected by topography artifacts, except for 180° phase jumps easily identifiable. Therefore the phase signal represents an ideal candidate for unambiguous assessment of genuine near-field scattering in the optical images.

ACKNOWLEDGMENTS

Partial financial support from the CNR-CNRS bilateral project “Diffusione Raman e Brillouin risonante e localizzazione spaziale di stati elettronici,” and from the Italy-Korea bilateral project E1 “Apertureless near-field scanning optical microscopy of single quantum systems and single molecules” is greatly acknowledged. This work was also supported in part by Korea Research Foundation Grant funded by Korea Government (MOEHRD, Basic Research Promotion Fund) (KRF-2005-070-C00054) (S.-C.H and S.-H.B) and in part by the Seoul R&D Program (S.-C.H). Nanotec is acknowledged for free software WSXM (www.nanotec.es).

- ¹F. Zenhausern, M. P. O’Boyle, and H. K. Wickramasinghe, *Appl. Phys. Lett.* **65**, 1623 (1994).
- ²R. Bachelot, P. Gleyzes, and A. C. Boccaro, *Appl. Opt.* **36**, 2160 (1997).
- ³R. Hillenbrand and F. Keilmann, *Appl. Phys. B: Lasers Opt.* **73**, 239 (2001).
- ⁴R. Hillenbrand, F. Keilmann, P. Hanarp, D. S. Sutherland, and J. Aizpurua, *Appl. Phys. Lett.* **83**, 368 (2003).
- ⁵S. Nie and S. R. Emory, *Science* **275**, 1102 (1997).
- ⁶D. Enders and A. Pucci, *Appl. Phys. Lett.* **88**, 184104 (2006).
- ⁷P. Mühlischlegel, H.-J. Eisler, O. J. F. Martin, B. Hecht, and D. W. Pohl, *Science* **308**, 1607 (2006).
- ⁸S. I. Bozhevolnyi, V. S. Volkov, E. Deveaux, J.-Y. Laulet, and T. W. Ebbesen, *Nature (London)* **440**, 508 (2006).
- ⁹B. Hecht, H. Bielefeldt, Y. Inouye, D. W. Pohl, and L. Novotny, *J. Appl. Phys.* **81**, 2492 (1997).
- ¹⁰M. Labardi, P. G. Gucciardi, M. Allegrini, and C. Pelosi, *Appl. Phys. A: Mater. Sci. Process.* **66**, S397 (1998).
- ¹¹P. G. Gucciardi and M. Colocci, *Appl. Phys. Lett.* **79**, 1543 (2001).
- ¹²R. Hillenbrand and F. Keilmann, *Phys. Rev. Lett.* **85**, 3029 (2000).
- ¹³M. Labardi, S. Patanè, and M. Allegrini, *Appl. Phys. Lett.* **77**, 621 (2000).
- ¹⁴L. Stebounova, B. B. Abramitchev, and G. C. Walker, *Rev. Sci. Instrum.* **74**, 3670 (2003).
- ¹⁵P. G. Gucciardi, G. Bachelier, A. Mlayah, and M. Allegrini, *Rev. Sci. Instrum.* **76**, 0361051 (2005).
- ¹⁶P. G. Gucciardi, G. Bachelier, and M. Allegrini, *J. Appl. Phys.* **99**, 1243091 (2006).
- ¹⁷J. Azoulay, A. Debarre, A. Richard, and P. Tchenio, *Appl. Opt.* **39**, 129 (2000).
- ¹⁸S. Patanè, P. G. Gucciardi, M. Labardi, and M. Allegrini, *Riv. Nuovo Cimento* **27**, 1 (2004).
- ¹⁹F. Formanek, Y. De Wilde, and L. Aigouy, *J. Appl. Phys.* **93**, 9548 (2003).
- ²⁰T. Taubner, F. Keilmann, and R. Hillenbrand, *Nano Lett.* **4**, 1669 (2004).

- ²¹L. Gomez *et al.*, J. Opt. Soc. Am. B **23**, 823 (2006).
- ²²B. Knoll and F. Keilmann, Opt. Commun. **182**, 321 (2000).
- ²³F. Formanek, Y. De Wilde, and L. Aigouy, Ultramicroscopy **103**, 135 (2005).
- ²⁴P. G. Gucciardi, M. Labardi, S. Gennai, F. Lazzeri, and M. Allegrini, Rev. Sci. Instrum. **68**, 3088 (1997).
- ²⁵P. M. Adam, J.-L. Bijeon, G. Viardot, and P. Royer, Opt. Commun. **174**, 91 (2000).
- ²⁶J. N. Walford *et al.*, J. Appl. Phys. **89**, 5159 (2001).
- ²⁷S. Diziain, D. Barchiesi, T. Grosjes, and P.-M. Adam, Appl. Phys. B: Lasers Opt. **84**, 233 (2006).
- ²⁸S. Hudlet *et al.*, Opt. Commun. **230**, 245 (2004).
- ²⁹D. R. Lide, *Handbook of Chemistry and Physics* (CRC, Boca Raton, FL, 2000).
- ³⁰Any further phase shift ϕ_1 , due, e.g., to the complex constant between the scattered and the incident fields, can be accounted in Eq. (3) by redefining ϕ_0 , as $\phi_0 = \phi_0 + \phi_1$.
- ³¹M. R. Spiegel and J. Liu, *Mathematical Handbook of Formulas and Tables*, 2nd ed. (McGraw-Hill, New York, 1999).
- ³²L. Billot *et al.*, Appl. Phys. Lett. **89**, 0123051 (2006).
- ³³A. Bek, R. Vogelgesang, and K. Kern, Rev. Sci. Instrum. **77**, 043703 (2006).